Measuring and Analyzing Transverse Low-Energy Ion Beam Emittances*

M. P. Stockli[1)]

(Spallation Neutron Source*, Oak Ridge National Lab, Oak Ridge, TN 37831, USA)

Abstract The transverse emittance of an ion beam describes its transverse size as the particles are transported from a source to a target. It allows for predicting beam losses in limiting apertures and the beam focus size at the target. Various definitions and issues are discussed. The most common and emerging measuring techniques are presented, including their advantages. Several methods of emittance data analysis, their accuracy and trustworthiness, are discussed.

Key words ion beams, ion beam transport, ion beam emittance, ion beam diagnostics, emittance analysis

1 Introduction

The normalized emittance of a charged particle beam is conserved along its axis of propagation (Liouville's theorem) as long as the particles are subjected to conservative forces, such as the electric and magnetic fields used for their transport[1]. Hence the emittance allows for designing minimum-loss beam transport systems and for predicting those losses. This is important for charged particle beam facilities in their quest for higher target yields, and essential for high-power accelerators where losses limit operation.

The transverse emittance is the four-dimensional distribution of all position coordinates along the two transverse configuration-space directions and their associated velocity coordinates. Sometimes emittances are given as volumes V_{xy} or as orthogonal, two- dimensional projections A_x and A_y that are occupied by a certain fraction of the beam. But most frequently, the emittances ε are given as semi-axis products of equal-area (/-volume hyper-) ellipses.

$$V_{xy}=\varepsilon_{xy}\cdot\pi^2\leqslant\varepsilon_x\cdot\varepsilon_y\cdot\pi^2/\chi=A_x\cdot A_y/\chi\ .$$

The equal sign applies for uncorrelated x and y coordinates. The shape-dependent form factor χ is about 2. Emittances are the product of a length and an angle with units of m·rad, mm·mrad, or simply m or μm. Semi-axes products are often given with the unit "π·m·rad," where π is a symbol and not a multiplier, which follows a rather unconventional suggestion[1]. Confusion is avoided by stating whether the given values represent volumes, areas, or semi-axis products.

The interest in emittance emerged with the development of accelerators, and several reviews have been published[1—4]. This paper gives a brief overview and an update on the most popular and emerging techniques for measuring and analyzing transverse emittances of low-energy charged-particle beams.

2 Measuring emittance areas

An adjustable lens and two beam profile monitors separated by a field-free drift length L, or alternatively two sets of adjustable slits and a large acceptance Faraday cup downstream of the second slit, are

Received 20 April 2007
∗ ORNL/SNS is managed by UT-Battelle, LLC, for the U.S. Department of Energy under contract DE-AC05-00OR22725
1) E-mail: stockli@sns.gov

sufficient to determine the emittance area occupied by a certain fraction of the beam, e.g. $\varepsilon_{90\%}$: while one set of slits is fully open, both jaws of the other set and the lens are tuned until the Faraday cup reads a 95% transmission through the smallest possible slit width $d_{\rm W}$, the diameter of the tuned beam waist.

Then, without further tuning, the open slit set is closed until each jaw reduces the current by 2.5%, yielding slit-opening d. According to the ellipse propagation equation[3—5], the 90% area emittance is

$$\varepsilon_{90\%} = d_{\rm W} \cdot (d^2 - d_{\rm W}^2)^{1/2} / (4 \cdot L) \ .$$

Alternatively, a more convenient procedure is available after the len's focal strength has been accurately characterized: the multi-gradient method determines the emittance area from the beam diameters measured with a single beam profile probe for different lens settings. Similarly, the multi-position method determines the emittance area from the beam diameters measured in different locations, if all the beam transport elements between the different locations have been accurately characterized. For both methods, three beam diameters are sufficient to determine the emittance area, while additional diameters allow for assessing its uncertainty[1, 4].

These methods measure the emittance area but provide no information on the distribution of the beam, and therefore do not allow for accurate predictions of losses. Low-energy beams especially benefit from measuring the distribution of the beam emittance, because their emittance ellipses are often distorted[4].

3 2-slit emittance scanners

Measuring 2-dimensional emittance distributions requires a slit to sample the beam position distribution and a downstream device to measure the trajectory angle distribution for each measured position. Low- energy beams are best sampled[6] with the slits shown in Fig. 1, where the slit taper angle $\theta_{\rm s}$ exceeds the maximum trajectory angle $x'_{\rm max}$ to keep the side of the slit in the shadow of the beam. This avoids grazing surface scattering, which changes the trajectory angles. Depending on the beam power, these slits may have to be actively cooled because either of them has to stop up to 100% of the beam. The stopping of ~99% of the beam on the front slits produces a copious amount of secondary electrons, normally exceeding the rate of the primary beam current, and exceeding the sampled beamlet current by several orders of magnitude. These electrons have rather small energies, rarely exceeding 20eV, and therefore can be easily controlled.

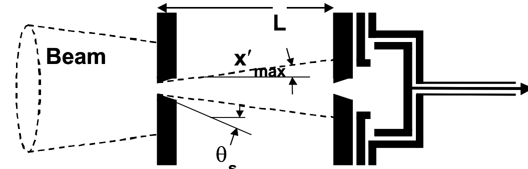

Fig. 1. Two slits and a fully shielded, suppressed Faraday cup yield accurate emittance distributions.

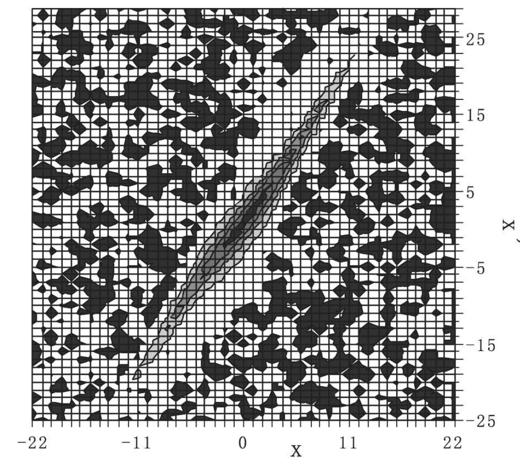

Fig. 2. Artifact-free emittance data from a 2-slit scanner.

Scanning the second slit and measuring the passing beam current with a Faraday cup measures the trajectory angle distribution of the sampled beamlet. The Faraday cup needs to be fully shielded to assure the exclusion of contributions from the secondary electrons produced by the discarded beam. In addition, the entrance to the Faraday cup needs to have a negatively-biased suppressor to prevent the escape of secondary electrons as well as to prevent low-energy electrons from entering. While secondary electrons are easily repelled, several hundred volts are normally preferred to assure the exclusion of electrons traveling with the beam such as convoy electrons ($E_{\rm e} \approx E_i \cdot m_{\rm e}/m_i$), as well as binary encounter

electrons ($E_e \approx 4 E_i m_e/m_i$), where E and m represent the ion and electron energy and mass as indicated by the subscripts, respectively. This produces artifact-free data as one can see in Fig. 2, where the beam current signals are surrounded by a background of noise with a random pattern of small positive (white) and small negative (black) signals[7].

4 Multi-collectors and wire harps

It takes a long time to measure the emittance distribution when precisely scanning two independent slits, because there are n·m position combinations needed for a distribution with n beam positions and m trajectory angles. Some scanners reduce the acquisition time by measuring the trajectory angle distribution with a wire harp or a multi-collector[4]. The small currents collected by the wires or collectors are converted by an array of amplifiers. Analog zeroing of the amplifiers leaves a small bias that varies among amplifiers, which should be eliminated by digitally zeroing each amplifier based on data obtained without real beam current.

It is common to apply a bias voltage to the wires or collectors. Applying a positive voltage prevents the escape of secondary electrons produced by the sampled beam, but allows for cross-talk between neighboring probes and can attract some of the many electrons generated by the discarded beam. Applying a negative voltage multiplies the signal from positive ions, while the signals from negative ions can decrease, vanish, or increase depending on the secondary electron emission coefficient. This coefficient depends on the properties of the ions and the surface, where the surface properties can change with beam exposure and time. In addition, an insufficient positive voltage (including zero or negative voltages) produces signals for intercepted photons and energetic neutral particles. These phenomena can create artifacts unrelated to the beam of interest and compromise the accuracy of the measurement. Fig. 3, for example, shows a beam probed with a slit and a multi-collector. The expanding beam is seen as dark, tilted ellipses, where a small flux of neutrals and/or photons produced the diagonal line.

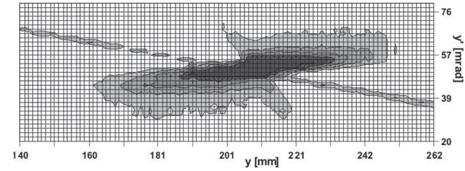

Fig. 3. Artifact infested data from a multi-collector.

5 Electric sweep- and allison-scanners

Electric scans can be significantly faster than mechanical scans and substantially reduce the data acquisition time. Several electric sweep scanners were developed that allowed for displaying the beam emittance instantaneously on an oscilloscope[8] as shown in Fig. 4. Electric sweep scanners are normally installed in separate beam lines due to the insertion length required for the three deflectors.

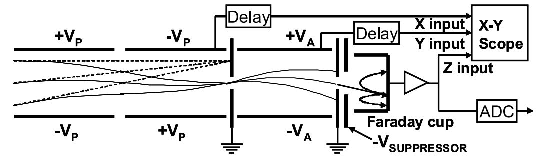

Fig. 4. Scopes display the emittance from electric sweeps.

Early in the 1980ies, Allison found a good compromise by combining an electric trajectory-angle sweep with a mechanical beam-position sweep[9]. Being reduced to a single deflector allows for mounting the entire scanner on a single motion feed-through and for insertion through a 15—20 cm-diameter port. Typical designs use a solid mounting base to assure an accurate alignment of the two slits, which is important for low-divergence beams.

Figure 5 shows an Allison scanner with an effective length L_{eff}[10] and a gap g between the deflector plates. Ions with an energy per charge of U and an angle x' require deflection voltages $\pm V$ of

$$V = 2 \cdot U \cdot x' \cdot (g/L_{\text{eff}}) \quad \text{or} \quad x' = V \cdot L_{\text{eff}}/(2 \cdot g \cdot U)$$

The gap limits the angular acceptance to $x'_{\max} = 2 \cdot g/L_{\text{eff}}$. Ideally, this matches the limit of the voltage supplies V_0, which leads to the design equation $V_0 \cong {x'_{\max}}^2 \cdot U_0$, where U_0 is the highest ion energy per charge and $x_{\max}$ the largest trajectory angle to be measured[11].

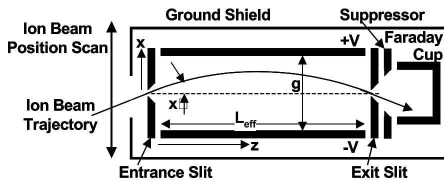

Fig. 5. Allison scanners scan trajectory angles electrically.

Ions backscattering from the deflector plates produce small artifacts[12] that can be eliminated by stair-casing the deflector plates with an angle $x'_{sc} = (8)^{1/2} \cdot g/L_{eff}$[11]. The results are artifact-free emittance data, as shown in Fig. 6.

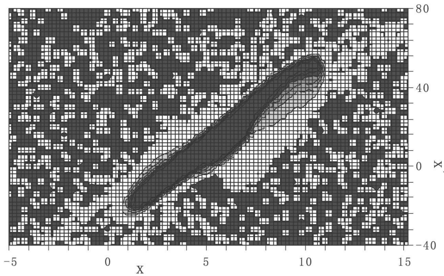

Fig. 6. Artifact free data from a stair-cased Allison scanner.

6 Pepper pot emittance scanners

Measured x, x' and y, y' emittance distributions of rectangular or elliptical beams yield a complete characterization for most beams. However, measuring the full 4-dimensional emittance x, y, x', y' can be beneficial for beams with highly complex distributions, such as ECRIS beams[13], as well as non-symmetric beams propagating through solenoids and non-sector dipole magnets, where the transverse magnetic force couples the x and y coordinates.

Four-dimensional distributions require $n_x \cdot n_y \cdot m_{x'} \cdot m_{y'}$ data to be acquired, which would take prohibitively long with standard scanners. As shown in Fig. 7, pepper-pot scanners circumvent the acquisition time problem by sampling a small, but regularly-distributed fraction of the beam with a pepper-pot plate and simultaneously measuring the dislocations of the many beamlets. The distance between the pepper-pot plate and the screen is normally adjustable to allow for sufficient transverse dislocation without overlapping images.

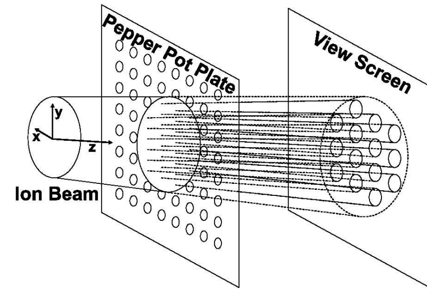

Fig. 7. Pepper pot scanners record 4-dimensional emittances.

Quantitative measurements were originally very time-consuming because they required photographic emulsions to be developed and analyzed[1]. The advent of small, high-resolution cameras with high-speed electronic read-outs rekindled interest in these scanners. Nowadays they can yield 4-dimensional emittance results in a split-second, which can eliminate cooling requirements[14]. If the beam is sufficiently large, pepper-pot emittance scanners yield incredibly detailed information on the beam emittance structure[13]. However, accurate emittance values remain a challenge because of the linearity of the recorded light level versus the incident beam current and the many artifacts that can be produced by the scattered light.

7 Extracting areas from distribution data

To correctly predict the transmission through tight collimators, their acceptance (hyper-) ellipses (or parallelograms) need to be fitted to the emittance data until the ellipses include the maximum possible current. This is cumbersome and of limited merit because the area of this ellipse is not subject to Louisville's conservation law. It is therefore simpler and more practical to evaluate areas with a perimeter following a constant current density i_f of the measured current distribution, because this area is conserved[1].

The true fraction needs to be calculated from the measured distribution by dividing the sum of the signals within the boundary by the sum of all signals.

It is important that the data have been digitally zeroed because a small bias can cause a significant error, due to the dominating majority of the signal-free background data[4]. However, most commonly the fraction f is expressed with respect to the maximum measured peak current i_{pk}, with $f=(1-i_f)/i_{pk}$. For Gaussian distributions this equals the fraction of the included current, but can significantly deviate for non-Gaussian distributions[4].

Area emittance values lack information on the shape, and are therefore of limited merit unless the emittance distribution is nearly elliptical.

8 RMS emittance analysis

The rms emittance calculates the "average distances from the center of the particle distribution in the position versus trajectory-angle phase space" and therefore is sensitive to the shape of the emittance boundary as well as to its distribution within the boundary. Rms emittances are conserved for linear forces that are proportional to the position coordinates x and y. Nonlinear forces that distort the emittance boundaries cause the rms emittance to increase[1], which make it a sensitive beam quality indicator:

$$E^x_{\mathrm{rms}} = \sqrt{\langle x^2\rangle \cdot \langle x'^2\rangle - \langle x\cdot x'\rangle^2},$$

with

$$\langle x^2\rangle = \frac{\sum\limits_{\mathrm{all}}(x-\bar{x})^2\cdot c(x,x')}{\sum\limits_{\mathrm{all}} c(x,x')}, \bar{x} = \frac{\sum\limits_{\mathrm{all}} x\cdot c(x,x')}{\sum\limits_{\mathrm{all}} c(x,x')},$$

$$\langle x'^2\rangle = \frac{\sum\limits_{\mathrm{all}}(x'-\bar{x}')^2\cdot c(x,x')}{\sum\limits_{\mathrm{all}} c(x,x')}, \bar{x}' = \frac{\sum\limits_{\mathrm{all}} x'\cdot c(x,x')}{\sum\limits_{\mathrm{all}} c(x,x')},$$

and

$$\langle x\cdot x'\rangle = \frac{\sum\limits_{\mathrm{all}}(x-\bar{x})\cdot(x'-\bar{x}')\cdot c(x,x')}{\sum\limits_{\mathrm{all}} c(x,x')},$$

To calculate the rms emittance (a semi-axes product) of complete distributions, a digital zeroing procedure is essential, because the dominating background data are multiplied with their (usually large) distance from the actual current distribution. In addition, it is beneficial, and sometimes required, to exclude all background far from the real distribution. Self-consistent methods provide quality assurance for the analysis of complete distributions[4, 7].

Artifacts often prohibit the use of self-consistent methods and one therefore has to resort to the use of a threshold. A thresholded Gaussian distribution has an rms emittance which is smaller by the same fraction as the threshold divided by the peak value. However, the fractional errors are much larger for most experimental distributions. An versatile analysis code is available[4].

References

1 Lejeune C, Aubert J. In: Applied Charged Particle Optics, Part A, A. Septier edt., Academic Press, New York, 1980, 159—259

2 Lichtenberg A J. Phase Space Dynamics of Particles, Wiley, New York, 1969

3 Sander O R. AIP Conf. Proc. 212, Melville, NY, 1991, 127—155

4 Stockli M P. AIP Conf. Proc. 868, Melville, NY, 2006, 25—62

5 Carey D C. The Optics of Charged Particle Beams, Harwood Academic Publishers, Chur, 1987

6 Stockli M P, Welton R F. PAC 2005, 2705—2707

7 Stockli M P, Welton R F, Keller R. Rev. Sci. Instrum., 2004, **75**: 1646—1649

8 Billen J H. Rev. Sci. Instrum., 1975, **46**: 33—40

9 Allison P W, Sherman J D, Holtkamp D B. IEEE Trans. Nucl. Sci., 1983, **NS-30**: 2204—2206

10 Wollnik H, Ewald H. Nucl. Instrum. Methods, 1965, **36**: 93—104

11 Stockli M P et al. AIP CP763, Melville, NY, 2005, 145—158

12 Stockli M P et al. AIP CP749, Melville, NY, 2005, 108—111

13 Späetke P et al. HEP & NP, 2007, **31**(Suppl. I): 192 (in Chinese)
(Späetke P 等. 高能物理与核物理, 2007, **31**(增刊 I): 192)

14 Hoffmann T et al. AIP CP546, Melville, NY, 2000, 432—439